Results in Physics 12 (2019) 975–981

Contents lists available at ScienceDirect

Results in Physics

journal homepage: www.elsevier.com/locate/rinp

Adsorption of binary polymer mixtures with different topology on a wall

Francis M. Gaitho*, Giuseppe Pellicane

School of Chemistry and Physics, University of Kwazulu-Natal, Private Bag X01, Scottsville, 3209 Pietermaritzburg, South Africa

ARTICLE INFO

2000 MSC:
41A05
41A10
65D05
65D17

Keywords:
Adsorption
Polymer architecture
Wall-fluid potential

ABSTRACT

We consider a binary mixture of two polymers with different architecture, consisting of linear and cyclic chains. We study this system by performing extensive molecular dynamics computer simulations of bead-spring models, which possess the open-chain and loop topology. The system is confined between two walls, and we consider both the case of attractive- and repulsive polymer-wall interactions. By changing the chain length of the two polymers so as to encompass two regimes with low and high degree of polymerization, we show the effect on the structural properties at the interface. Our results provide some physical insight on the competition between polymer architecture and chain length in determining the surface adsorption.

Introduction

Techniques for surface modification of materials are important for industrial applications especially in coatings, adhesives, and biological engineering. A possible way of achieving such modification is through the blending of two different polymers. As a result, the surface will carry the desirable characteristics of one of the components, while at the same time exhibiting features peculiar to the combination of the two chemical species. Additionally, in many applications polymer blends occur in the form of a thin film geometry, where the surface properties at the interface of the film components become even more important [1–4]. The role played by the different topology of the two polymers is also an area of current investigation, as for instance in photovoltaic devices, where elongated polymers and compact fullerenes are blended, and the way they get structured close to the electrode can influence their charge separation, and the overall efficiency of the device [5–7]. Several experimental studies have shown that the miscibility of polymer blends depends on molecular weight and chain architecture [8,9]. Recently, we extensively investigated how the chain topology of the two components determines the surface behaviour in the case of low-energy interfaces, which are for example achieved by exposing the polymer blend to vacuum [10–12]. However, there is a limited amount of studies unveiling the structural features of surface adsorption of polymer blends under the effect of wall potentials, and the existing studies do not focus on the role played by the chain length and the different topology of the two polymers [13–20]. Therefore, a fundamental understanding of how the competition between interpolymer forces and polymer-wall forces determines surface behavior is lacking, and computational studies in this direction might be helpful to fill the knowledge gap. Besides the specific interest in polymer science, a general understanding of structural properties in the presence of geometrical constraints is useful for many colloidal [21–23] or biological [24] fluid materials. In this paper, we consider binary mixtures of ring and linear polymers with the same repeat chemistry, which are confined between both attractive and repulsive planar walls. Our main goal is to understand how the topology and molecular mass of the two polymer species alter the adsorption at the interface. For this reason, we consider a coarse-grained model of polymer blends with two very different chain lengths, which are meant to represent the case of low degree of polymerization, namely $N_b = 10$ monomers per polymer, and the case of high degree of polymerization, $N_b = 100$ monomers per polymer.

The paper is organized as follows. In the next section, we discuss the model and the methods adopted. Then, in the third section, we present the results and discussion. Finally, in the last section, we report our conclusions.

The model

In this paper, we use the bead-spring model by Kremer and Grest [25] to study a binary mixture of linear and cyclic polymers, each having beads (monomers) of equal mass m_i and connected to the neighbouring ones by bonded pair potentials. The bonded interaction is represented by the finitely extensible non-linear elastic (FENE) [25,26]

* Corresponding author.
E-mail addresses: fgaitho@mmust.ac.ke (F.M. Gaitho), pellicane@ukzn.ac.za (G. Pellicane).

https://doi.org/10.1016/j.rinp.2018.12.042
Received 11 October 2018; Received in revised form 20 November 2018; Accepted 9 December 2018
Available online 16 December 2018

potential:

$$U_{fene}(r) = \begin{cases} -0.5Kr_0^2\ln\left[1-\left(\frac{r}{r_0}\right)^2\right] + L_{lj_{12-6}}, & r \leqslant r_0 \\ -0.5Kr_0^2\ln\left[1-\left(\frac{r}{r_0}\right)^2\right] & r > r_0 \end{cases} \quad (1)$$

where $K = 30\,\epsilon/\sigma^2$, $r_0 = 1.5\sigma$ is the maximum possible distance between two consecutive beads, and $L_{lj_{12-6}}$ is the Lennard-Jones 12-6 potential. In this model, the total external force acting on the beads of the polymer chains, excluding for the moment the polymer-wall interactions, is given by;

$$F^{tot} = F_B + F_S + F_{LJ_{12-6}}, \quad (2)$$

where F_B, F_S, F_E are the Brownian force, the Stokes's drag, and the force originating from the Lennard-Jones 12-6 potential, respectively. The Brownian force represents random collisions of beads at temperature T, and is expressed as

$$F_B = \sqrt{\frac{k_B T m}{\delta t \psi}}, \quad (3)$$

where k_B is the Boltzmann constant, m is the mass of the bead, δt is the time-step, and ψ is the damping constant of the Langevin thermostat [27]. Stokes's drag provides viscous damping on a bead of velocity V according to the force

$$F_S = -\left(\frac{m}{\psi}\right)V. \quad (4)$$

The interactions between non-bonded beads are taken into account via the Lennard-Jones 12-6 potential, that is truncated and shifted at the cut-off distance $r_c = 2.5\sigma$:

$$U_{lj_{12-6}}(z) = \begin{cases} 4\,\epsilon\left[\left(\left(\frac{\sigma}{r}\right)^{12} - \left(\frac{\sigma}{r}\right)^6\right) + \frac{1}{4}\right], & r \leqslant r_c \\ 0 & r \geqslant r_c \end{cases} \quad (5)$$

where σ and ϵ are, respectively, the LJ distance and energy parameters. Finally, the polymer beads are interacting with a flat surface perpendicular to the z-direction of the simulation box. We considered the case of attractive LJ polymer-wall interactions:

$$U_{lj_{9-3}}(z) = \epsilon\left[\frac{2}{15}\left(\frac{\sigma}{z}\right)^9 - \left(\frac{\sigma}{z}\right)^3\right], \quad z < r_{cw} \quad (6)$$

where $U_{lj_{9-3}}(z)$ is the Lennard-Jones 9-3 potential, z is the distance of the beads from the wall, and r_{cw} is the distance at which the bead and the wall will no longer interact. The energy of the wall potential is shifted so that the wall-bead interaction is zero at the cutoff distance $r_{cw} = 2\sigma$. In the case of repulsive walls we used only the repulsive part of the Lennard-Jones 12-6 potential reported in Eq. (5), by shifting the potential at the distance $z = 2^{1/6}\sigma$ of the energy minimum, so that the wall-bead interaction is zero at that distance [15,28]. We performed molecular dynamics simulation [29] of our model by using the Large-scale Atomic/Molecular Massively Parallel Simulator (LAMMPS) package [30]. In all our simulations, we kept the reduced temperature $T^* = k_B T/\epsilon = 1$. The constant ψ, and time-step size δt, were set to $2\tau^{-1}$ and 0.005τ, respectively, where $\tau = \sigma(m/\epsilon)^{1/2}$. We generated initial configurations for binary mixtures of linear and cyclic polymers of two different chain lengths: $N_b = 10, 100$ beads per chain, at equimolar composition, that is, $C_0 = \frac{N_l^0}{(N_c^0 + N_l^0)}\cdot 100 = 50\%$, where N_l^0 and N_c^0 are the total number of linear and cyclic chains in the simulation box. We studied systems with a total number of beads $N_l^0 + N_c^0 = 200,000$. The initial configurations were generated by positioning the centers of mass of each polymer on the sites of a parallepiped lattice, that was elongated along the z-direction. The initial lattice had a large lattice parameter in order to prevent overlaps between neighbouring polymers. An energy minimization procedure was run on the initial configuration, and then we shrank isotropically the volume of the initial simulation box using the LAMMPS/deform procedure. Subsequently, we perfomed constant-pressure (NPT) molecular dynamics simulations for 1.0×10^7 MD timesteps at atmospheric pressure and reduced temperature $T^* = 1$, using respectively, a Berendsen barostat and a Langevin thermostat [31]. These simulations were performed with full periodic boundary conditions (PBCs) along x-, y- and z-directions. Then, we removed the PBCs only along the z-direction, so as to expose the binary polymer blend to two walls at low and high z values, while at the same time rebuilding the broken polymers across the z-direction. We then performed 5.0×10^7 MD steps in the NPT ensemble to relax the systems, followed by production runs in the NVT ensemble of 10^8 MD steps. The structural properties of the polymer films reported in the next section, were studied as a function of the distance from the wall, along the z-direction. In the subsequent part of the paper, we will average the value of physical quantities as measured starting from each of the two walls.

Results and discussion

Besides simulating the blended system, we also simulated the pure components in the presence of the wall, so as to understand how the polymer interactions, which are driven by the different topology of the two species, influence the adsorption properties. The two local densities ρ_l for linear species, and ρ_c for cyclic species, for the binary mixture are defined as

$$\rho_{(l,c)} = \frac{N_{(l,c)}}{V}, \quad (7)$$

where $N_{(l,c)}$ is the number of particles of linear/cyclic polymer species contained in a slab of thickness σ along the z-direction, and V is the volume of that slab. Similarly, the same quantities for the pure components are indicated as

$$\rho_{(lP,cP)} = \frac{N_{(lP,cP)}}{V}. \quad (8)$$

Variations of the density $\rho(z)$ for blends of cyclic-linear polymer blends are considered for the two chain lenghts 10-mers and 100-mers, respectively, and then scaled with respect to their bulk value $\rho^0(z)$. Here and in the subsequent discussion, we will refer to the *bulk* value of any quantity, as the value that the quantity achieves in the middle of the simulation box, far away from the two walls. Values of scaled densities, $\rho(z)/\rho^0(z)$, as function of distance $z^* = z/\sigma$ from the wall are presented in Figs. 1 and 2. The bulk values of the densities are reported in Tables 1 and 2. The similarities of the bulk density values demonstrate that in the middle of the simulation box, these values are detached from the nature of the inhomogeneity at the interface (either the attractive, or repulsive walls). If we look at the left panels of both figures, where the results for attractive polymer-wall interactions are reported, we notice that regardless of the chain length, these interactions are not strong enough to make the polymer concentration nearby the interface higher than the *bulk* value. However, while for short chains (Fig. 1), the pure components are more adsorbed at the wall, it is the opposite for long chains (Fig. 2). Still in the pure case, linear polymers are only slightly more adsorbed at the wall than cyclic polymers for short chains (Fig. 1), while for long chains, the two species exhibit a similar adsorption (Fig. 2). However, it is interesting to note that, while for short chains linear and cyclic polymers exhibit a similar adsorption (Fig. 1), in the long-chain case, the density of linear polymers get clearly far more increased at the interface (Fig. 2). Before we provide a possible explanation for the enhancement of linear chains at the surface, we notice that the effective flexibility of the two type of chains can be measured by counting the number of conformations achievable by them, which is obviously different for the closed and open topologies exhibited by cyclic and linear chains, respectively. Then, this effect (enhancement of linear chains) might be driven by the higher flexibility

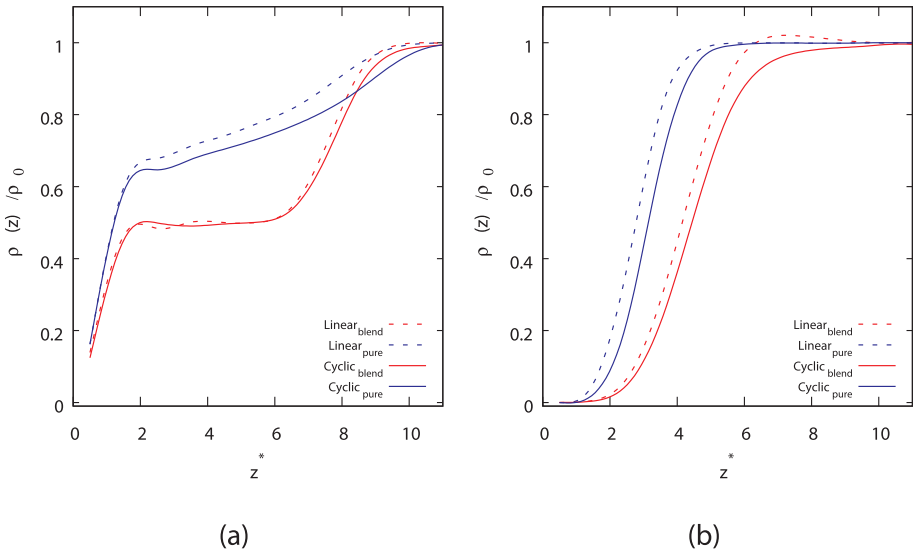

Fig. 1. Scaled density for 10-mers as a function of distance from (a) attractive wall and (b) repulsive wall.

of linear chains, which allows them to better maximize the number of their contacts (energetic interactions) with the wall. On the other hand, what we observe is also a clear signature of the way the different topology (entropy) of the two polymers is able to enhance one of them at the expenses of the other species, nearby the interface. Enhancement of linear chains was also observed by Yethiraj when linear-branched polymer attractive interactions were switched-off [32]. If we look at the right panels of Figs. 1 and 2 (repulsive polymer-wall interactions), we notice that even in this case the pure systems are more enhanced for short chains than the blended ones (Fig. 1), while the opposite happens for long chains (Fig. 2). In both the pure and blended cases we observe that at low chains, linear polymers are more adsorbed nearby the wall (Fig. 1), while the density of cyclic polymers get more increased at the interface when we consider the case of long chains (Fig. 2). This behaviour is similar to what we already reported for the case of a polymer-vacuum interface, suggesting that repulsive or neutral polymer-interface interactions produce similar effects.

In order to get more insight into the observed density behaviour, we calculated the radius of gyration of the two polymer species, which quantifies the chain configurational changes at the wall. The mean square radius of gyration R_g of the chains in terms of the degree of

Table 1
Bulk densities for polymer films – attractive wall.

Bulk density	10-mers	100-mers
$\rho^0_{c_B}$	1.78	1.98
$\rho^0_{c_P}$	3.56	3.57
$\rho^0_{l_B}$	1.75	1.59
$\rho^0_{l_P}$	3.47	3.56

Table 2
Bulk densities for polymer films – repulsive wall.

Bulk density	10-mers	100-mers
$\rho^0_{c_B}$	1.78	1.73
$\rho^0_{c_P}$	3.56	3.57
$\rho^0_{l_B}$	1.75	1.84
$\rho^0_{l_P}$	3.48	3.56

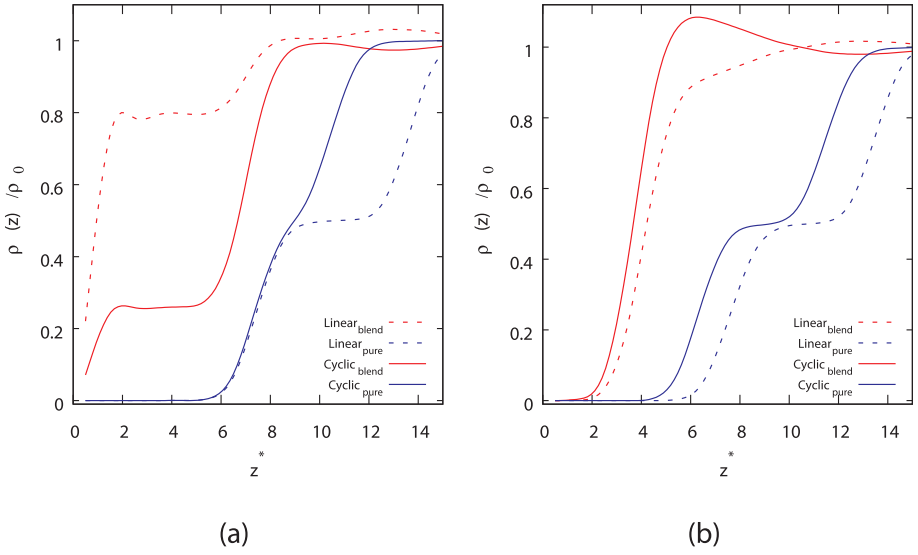

Fig. 2. Scaled density for 100-mers as a function of distance from (a) attractive wall and (b) repulsive wall.

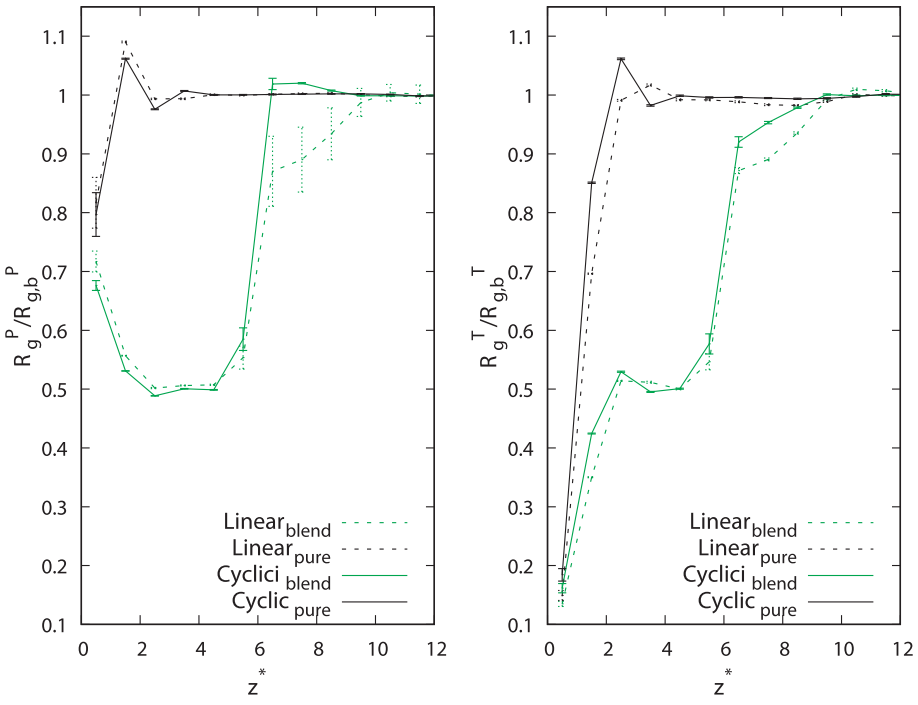

(a)

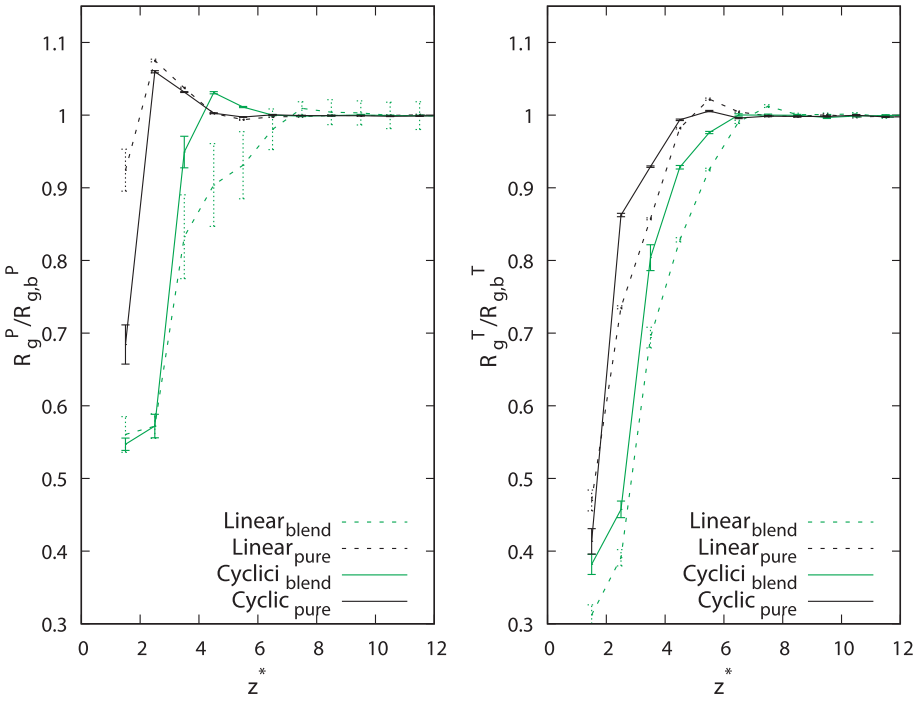

(b)

Fig. 3. Parallel (left panels) and perpendicular (right panels) radius of gyration for 10-mers as a function of distance from (a) attractive wall and (b) repulsive wall.

polymerization N_b is given by:

$$\langle \bar{R_g} \rangle = \sqrt{\left\langle N^{-1} \sum_{i}^{N_b} (\bar{R_i} - \overline{R}_{com})^2 \right\rangle}, \tag{9}$$

where N is the total number of beads per polymer, $R_{com}(t)$ is the position of the center of mass of the whole chain and $R_i(t)$ is the position vector of each atom in a chain, at time t. The existence of a planar interface prompt us to look at the two components of $R_g(t)$, which are parallel and perpendicular to the wall(s):

$$\bar{R_g^P} = \sqrt{\left\langle \frac{1}{N} \sum_{i=1}^{N} [(x_i(t) - x_{com}(t))^2 + (y_i(t) - y_{com}(t))^2] \right\rangle} \tag{10}$$

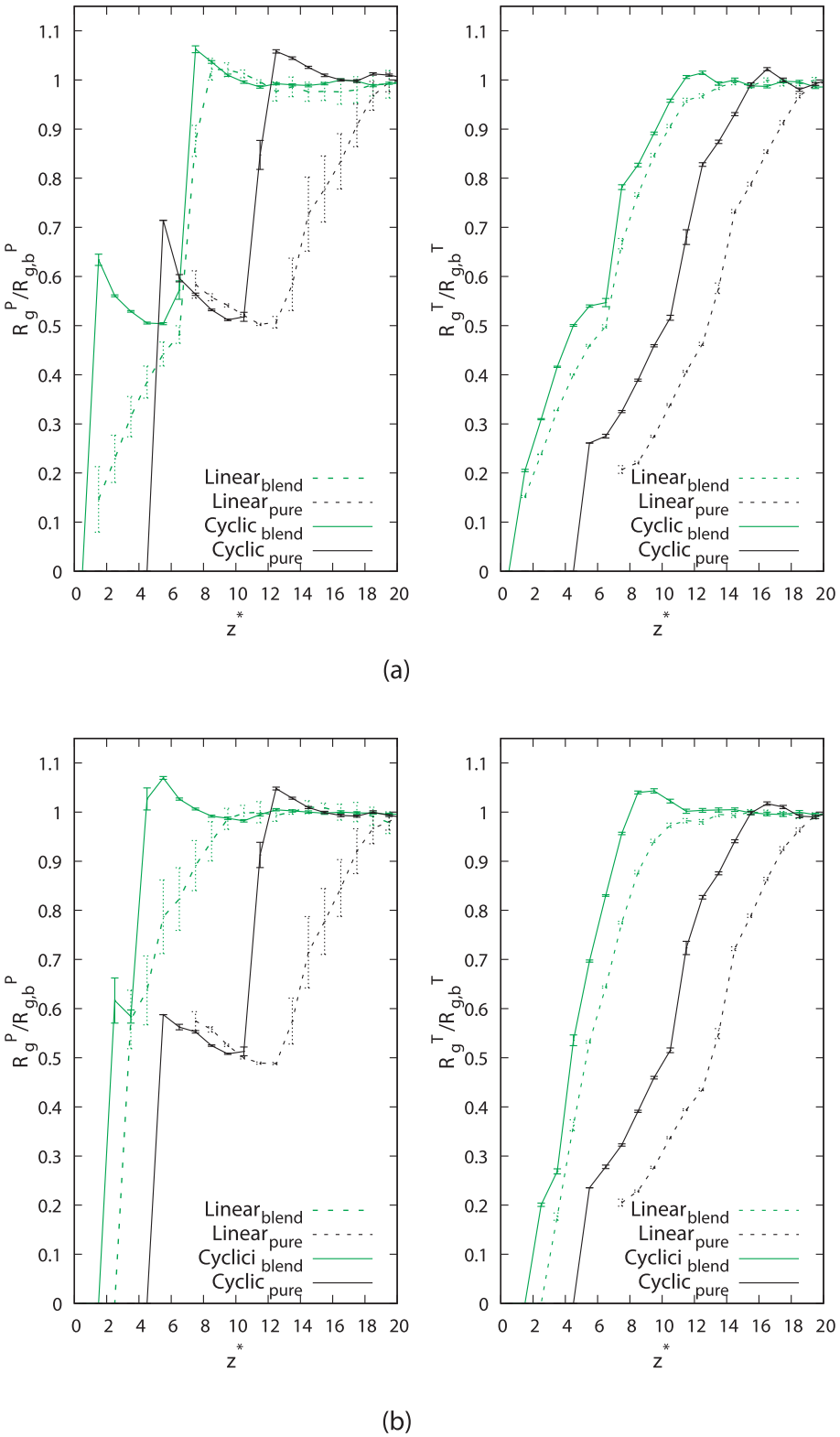

Fig. 4. Parallel (left panels) and perpendicular (right panels) radius of gyration for 100-mers as a function of distance from (a) attractive wall and (b) repulsive wall.

$$\bar{R_g^T} = \sqrt{\left\langle \frac{1}{N}\sum_{i=1}^{N}(z_i(t) - z_{com}(t))^2 \right\rangle} \tag{11}$$

The bulk normalized components of R_g, i.e. R_g^P and R_g^T, are shown as a function of distance from the interface z^* in Figs. 3 and 4, for 10-mers and 100-mers, respectively. The bulk values of R_g^P and R_g^T as well as their combined (3D) values are reported in Tables 3 and 4. Similarly as it was observed for the local densities, the almost identical values of the quantities reported in these tables show that, in the middle of the simulation box, the system is not perturbed by the presence of the walls.

If we look at the results reported in Fig. 3 for small chains, we realize that the R_gs of the blended components tend to be lower at the interface than their pure counterparts for the case of the attractive wall (see top panels of Fig. 3). There are minimal differences between the

Table 3
Bulk average radii of gyration for polymer films of 10-mers and 100-mers; attractive wall.

Polymer system	10-mers			100-mers		
	$R_{g,b}^{3D}$	$R_{g,b}^{P}$	$R_{g,b}^{T}$	$R_{g,b}^{3D}$	$R_{g,b}^{P}$	$R_{g,b}^{T}$
Cyclic_{Blend}	1.14	0.66	0.64	3.62	2.08	2.05
Cyclic_{Pure}	1.14	0.65	0.64	3.50	2.00	1.97
Linear_{Blend}	1.44	0.81	0.79	5.00	2.87	2.72
Linear_{Pure}	1.44	0.82	0.79	5.11	2.89	2.84

Table 4
Bulk average radii of gyration for polymer films of 10-mers and 100-mers; repulsive wall.

Polymer system	10-mers			100-mers		
	$R_{g,b}^{3D}$	$R_{g,b}^{P}$	$R_{g,b}^{T}$	$R_{g,b}^{3D}$	$R_{g,b}^{P}$	$R_{g,b}^{T}$
Cyclic_{Blend}	1.14	0.66	0.64	3.65	2.09	2.04
Cyclic_{Pure}	1.14	0.65	0.64	3.51	2.02	2.00
Linear_{Blend}	1.44	0.81	0.79	5.10	2.86	2.83
Linear_{Pure}	1.45	0.82	0.80	5.07	2.88	2.85

two polymer species, suggesting that both polymers tend to be more compressed at the interface when they are mixed together, than when they are alone. In the case of the repulsive wall, the differences between the pure and the blended cases are smaller, but still the blended polymers are slightly more packed at the interface (see bottom panels of Fig. 3). If we interpret both this result and the one reported in Fig. 1, we can conclude that in the case of short chains, polymers get more depleted and more efficiently squeezed in the presence of attractive polymer-wall interactions. The similarity of the R_g profiles of the two species was already observed for small chains, in the absence of a hard interface [12]. In general, the polymer sizes tend to get smaller when the wall is approached, regardless of the nature of the wall, with the only exception of the parallel component of R_g for the attractive wall, that appears to grow very close to the interface (see left panel of Fig. 3(a)). In the limit of long chains, we observe that blended systems keep a larger R_g than their pure counterparts (see Fig. 4). While in the presence of an attractive wall, there aren't remarkable differences in the two components of R_g for the two polymer species (see top panels of Fig. 4), cyclic chains in the presence of a repulsive wall appear to possess larger values of R_g^P and R_g^T. Finally, in Figs. 5 and 6, we report the total and self average energy per polymer. The self energy represents the energy contribution originating from self-interactions within the same polymer species. In the case of short chains (Fig. 5), we observe that regardless of the nature of the wall, the total and self energies of linear polymers are always lower than their counterparts of cyclic chains. However, the gap between them tends to become smaller when the repulsive wall is approached (see right panel of Fig. 5). The likely reason for that is the absence of attraction between the polymers and the wall when the purely repulsive wall is considered, which does not interfere with the energetic contacts between polymer beads. The lower energies observed for linear polymers (blue and red lines in the two panels of Fig. 5), and the comparable gaps between total and self energies of the two polymers (gap 1: blue versus green line; gap 2: red versus black line), suggest that linear polymers are able to better maximize their number of pair interactions because of their higher flexibility as compared to cyclic polymers. Similarly as it was observed for free-standing polymer blends [12,11], the loop geometry of cyclic chains emerges as a tight constraint for low degrees of polymerization. For the case of long chains (Fig. 6), the total energies of the two polymer species are very similar (blue and green lines almost overlap with each other), while the repulsive wall is able to increase the self-interactions among cyclic chains to the point that their self-energy is lower than the corresponding one for linear chains (see right panel of Fig. 6: black versus red line). The similarity of the total energies per polymer is to be expected when the two polymer species are long enough because their flexibility becomes also similar.

The lower self-energies achieved by cyclic chains in the presence of the repulsive wall can be explained in terms of the larger sizes which are achieved by them, when they approach the interface (see right panel of Fig. 4(b)), and also because they are more concentrated therein (see Fig. 2(b)). It is interesting to note that the pure systems show overlapping total and self energies (see dashed lines of Figs. 5,6), indicating that our observations are a genuine result of blending polymers with very different architecture, ultimately pointing to the important role of entropic effects in determining surface adsorption for these systems.

Conclusions

We studied a coarse-grained model for a polymer blend with cyclic and linear chains by using molecular dynamics computer simulations. Our model was exposed to both attractive and repulsive walls, while the

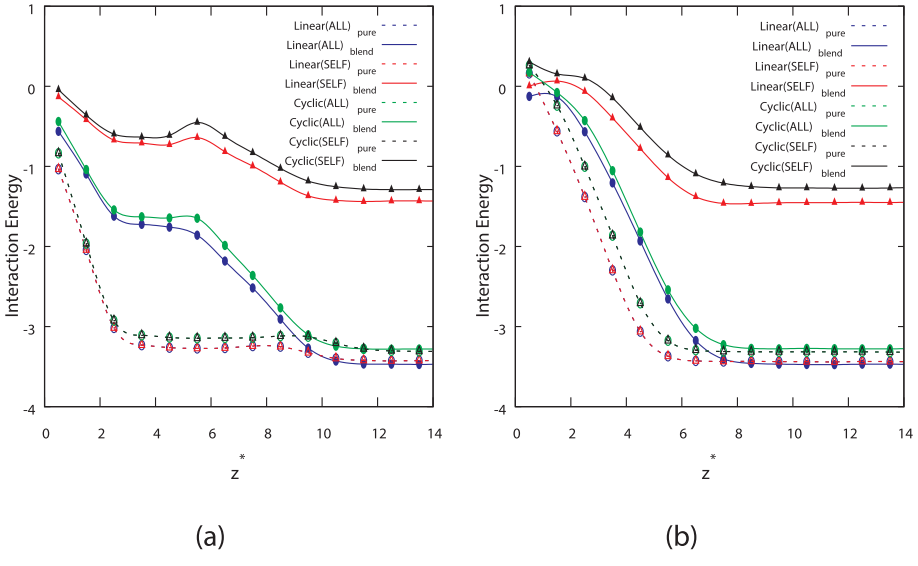

Fig. 5. Interaction energy for polymer films of 10-mers as a function of distance from (a) attractive wall and (b) repulsive walls.

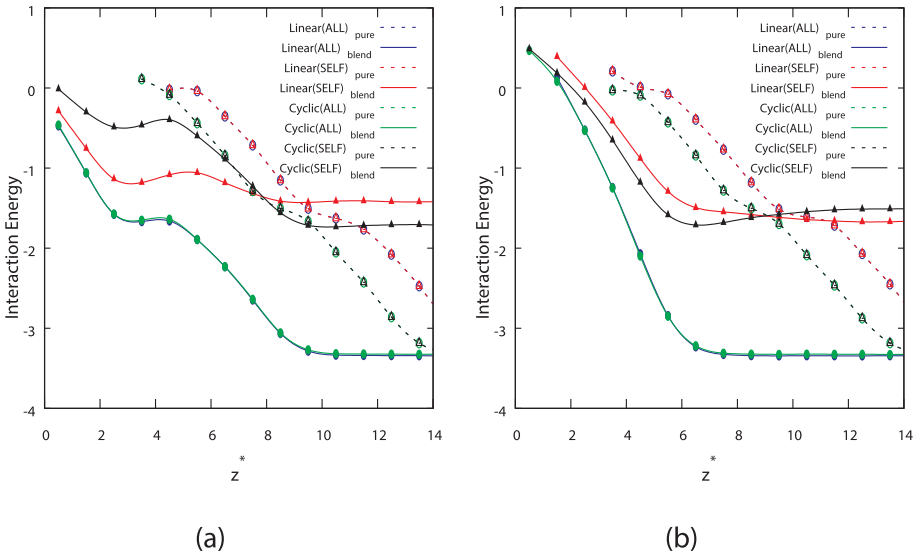

Fig. 6. Interaction energy for polymer films of 100-mers as a function of distance from (a) attractive wall and (b) repulsive walls.

strength of polymer-polymer interactions was kept similar to the one of polymer-wall interactions. We considered both short ($N_b = 10$) and long chains ($N_b = 100$), which allowed us to understand the role of topology and polymer weight in determining the surface properties of the model. We found that in the presence of favourable (attractive) polymer-wall interactions, for short chains, linear and cyclic polymers have similar adsorption features, while in the long-chain case, the density of linear polymers get clearly far more increased at the interface. We identified the higher flexibility of linear chains as a possible reason for this effect. In the presence of repulsive polymer-wall interactions, when considering short chains, linear polymers are more adsorbed nearby the wall, while the density of cyclic polymers get more increased at the interface in the case of long chains. This behaviour is similar to the one observed for free-standing polymer films [12]. Our results provide evidence of the way the differences in the topology of the polymer chain are able to enhance one polymer species, at the expenses of the other one, nearby the interface. We will try to understand how the dynamical properties get affected by polymer architecture, as well as the threshold between different regimes upon changing the chain length, in a forthcoming study.

Acknowledgments

G. P. and F. G. acknowledge the National Research Foundation (NRF) of South Africa for financial support through Grants No. 106020 and 114907, and the Centre for High Performance Computing (CHPC) at CSIR (South Africa).

Appendix A. Supplementary data

Supplementary data associated with this article can be found, in the online version, athttps://doi.org/10.1016/j.rinp.2018.12.042.

References

[1] Teng CY, Sheng YJ, Tsao HK. Boundary-induced segregation in nanoscale thin films of athermal polymer blends. Soft Matter 2016;12:4602.
[2] Kerstin M, Bugnicourt E, Latorre M, Jorda M, Echegoyen YS, Lagaron JM, et al. Review on the processing and properties of polymer nanocomposites and nanocoatings and their applications in the packaging. Autom Solar Energy Fields Nanomater 2017;74:2–47.
[3] Arbab EAA, Mola GT. V2O5 thin film deposition for application in organic solar cells. Appl Phys A: Mater Sci Process 2016;122:1–8.
[4] Oseni SO, Mola GT. The effect of uni-and binary solvent additives in PTB7:PC61BM based solar cells. Solar Energy 2017;150:66–72.
[5] Vithanage DA, Devižis A, Abramavičius V, Infahsaeng Y, Abramavičius D, MacKenzie RCI, et al. Visualizing charge separation in bulk heterojunction organic solar cells. Nat Commun 2013;4:2334.
[6] Lu L, Luping Y. Understanding low bandgap polymer PTB7 and optimizing polymer solar cells based on it. Adv Mater 2014;26:4413–30.
[7] Gaitho FM, Mola GT, Pellicane G. Computational approach to the study of morphological properties of polymer/fullerene blends in photovoltaics. Phys Sci Rev 2018;3(2):13–25.
[8] Gustavo AS, Cangialosi D. Describing the component dynamics in miscible polymer blends: towards a fully predictive model. J Chem Phys 2006;124:154904 .
[9] Huan W, Shentu B, Faller R. Molecular dynamics of different polymer blends containing poly(2,6-dimethyl-1,4-phenylene ether). Phys Chem Chem Phys 2015;17:4714.
[10] Gaitho FM, Tsige M, Mola GT, Pellicane G. Surface segregation of cyclic chains in binary melts of thin polymer films. Influence Const Concentr Polym 2018;10(324):1–16.
[11] Tchoukouegno MM, Gaitho FM, Mola GT, Tsige M, Pellicane G. Unraveling the surface composition of symmetric linear-cyclic polymer blends. Fluid Phase Equilbr 2017;441:33–42.
[12] Pellicane G, Tchoukouegno MM, Mola GT, Tsige M. Surface enrichment driven by polymer topology. Phys Rev E 2016;93:050501(R).
[13] Bhatia QS, David Pan H, Jeffrey T. Koberstein Preferential surface adsorption in miscible blends of polystyrene and poly(vinyl methyl ether). Macromolecules 1988;21(7):2166–75.
[14] Baschnagel J, Binder K. On the influence of hard walls on structural properties in polymer glass simulation. Macromolecules 1995;28(20):6808–18.
[15] Sijia L, Wanxi Z, Weiguo Y, Tongfei S. Structure and dynamics of confined polymer melts from attractive interaction to repulsive interaction between polymer and smooth wall. Chem Res Chin Univ 2015;31(3):477–83.
[16] Marcus M. Matyjaszewski Kris, Müller Martin, editors. Polymers at interfaces and surfaces and in confined geometries. Comprehensive Polymer Science, vol. 1. 2011. p. 1–42.
[17] Muller M, Albano EV, Binder K. Symmetric polymer blend confined into a film with antisymmetric surfaces: interplay between wetting behavior and the phase diagram. Phys Rev E 2000;62:5281–95.
[18] Bitsanis I, Hadziioannou G. Molecular-dynamics simulations of the structure and dynamics of confined polymer melts. J Chem Phys 1990;92:3827–47.
[19] Veress KD, Forrest JA, Dutcher JR. Mechanical confinement effects on the phase separation morphology of polymer blend thin films. Phys Rev E 1998;57:5811–7.
[20] Ziebarth JD, Wang Y. Interactions of complex polymers with nanoporous substrate. Soft Matter 2017;12:5245–56.
[21] Pellicane G, Vink RLC, Caccamo C, Lowen H. Colloid-polymer mixtures in the presence of quenched disorder: a theoretical and computer simulation study. J Phys Condens Matter 2008;20(11). 115101.
[22] Pellicane G. Colloidal model of lysozyme aqueous solutions: a computer simulation and theoretical study. J Phys Chem 2012;116(11):2114.
[23] Pellicane G, Pandaram OD. Gibbs ensemble Monte Carlo of nonadditive hard-sphere mixtures. J Chem Phys 2014;141(4):044508 .
[24] Pellicane G, Cavero M. Theoretical study of interactions of BSA protein in a NaCl aqueous solution. J Chem Phys 2013;138(11):115103 .
[25] Grest GS, Kremer K. Molecular dynamics (MD) simulations for polymers. Phys Rev A 1986;33:3628.
[26] Kremer K, Grest GS. Molecular dynamics (MD) simulations for polymers. J Comput Phys 1990;117:5057.
[27] Samoletov AS, Dettmann CP, Chaplain MAJ. Thermostats for “slow” configurational modes. J Stat Phys 2007;128:1321–36.
[28] Weeks JD, Chandler D. Role of repulsive forces in determining the equilibrium structure of liquids. J Chem Phys 1971;54(12):5237–47.
[29] Abramo MC, Caccamo C, Calvo M, Conti Nibali V, Costa D, Giordano R, et al. Molecular dynamics and small-angle neutron scattering of lysozyme aqueous solutions. Philos Magn 2011;91(SI:13–15):2066–76.
[30] Plimpton SJJ. Chem Phys 1995;117:1.
[31] Berendsen HJC, Postma JPM, van Gunsteren WF, DiNola A, Haak JR. Molecular dynamics with coupling to an external bath. J Chem Phys 1984;81(8):3684–90.
[32] Yethiraj A. Entropic and enthalpic surface segregation from blends of branched and linear polymers. Phys Rev Lett 1995;74(11):1–4.